A Two-Dimensional Model of Inertial Oscillations Generated by a Propagating Wind Field

PIJUSH K. KUNDU

Nova University, Oceanographic Center, Dania, FL 33004

(Manuscript received 12 November 1985, in final form 10 February 1986)

ABSTRACT

A linear, two-dimensional, continuously stratified, viscous model has been developed to study the inertial oscillations generated by a propagating wind field. The model, an extension of that of Kundu and Thomson, includes the presence of a coast and superposition due to distributed forcing. These two effects generate a large subsurface oscillation, provided the wind spectrum has energy near the inertial frequency. The presence of the coast causes an additional blue shift of the frequency, and a downward flux from the surface–coast corner. The superposition of responses with random phases does not cancel out but initially increases the rms amplitude as (time)$^{1/2}$. The model spectra have a blue shift that increases with depth and can also contain secondary peaks at higher frequencies if the speed of propagation is not too large. For a given propagation speed the blue shift, and hence the downward flux from the surface, is larger in the deep ocean where the gravity wave speeds c_n are larger. A calculation in the open ocean with a thermocline shows a decrease of the inertial oscillations with depth, and a clear upward phase and downward energy propagation. Although the model subsurface oscillations are large enough to explain the observations, they are too highly correlated in the vertical and horizontal directions. It is suggested that the variations perpendicular to the direction of propagation, and the β-effect, should be included in the model in order to explain the incoherence of the observed oscillations.

1. Introduction

Inertial oscillations, with a frequency close to the Coriolis frequency, are observed almost everywhere in the ocean. While their surface magnitudes can be explained by the wind forcing, the source of subsurface oscillations has not been adequately explained. Pollard (1970) studied an open ocean model due to a "switched-on" (that is, step input in time) spatially varying wind and concluded that the subsurface amplitudes were too low to explain the observations. Kundu et al. (1983) studied a coastal model and forced it with a switched-on spatially uniform alongshore wind. The vanishing normal velocity condition resulted in a decay of the oscillations near the coast (coastal inhibition), forcing a downward flux of inertial energy from the surface-coast corner. However, the maximum subsurface amplitude was less than 1 cm s^{-1} due to a 1 dyn cm^{-2} wind.

In a later calculation, Kundu (1984) argued that one possible way to increase the subsurface oscillations, without proportionally increasing the surface oscillations, is to abandon the switched-on forcing and apply a continually varying wind having energy around the inertial frequency. It was shown that the mean square response at time t due to a completely random forcing is

$$\overline{u^2}(t) = 2\pi S_\tau \int_0^t u_\delta^2 dt, \qquad (1)$$

where S_τ is the spectrum of the wind stress, and u_δ is the response due to an impulsive forcing and therefore equals the time derivative of the step response. Equation (1) shows that the responses due to a superposition of uncorrelated steps do not cancel out, but makes the rms response initially increase as $t^{1/2}$, as in the random walk problem. It also shows that the rms response reaches stationarity in the decay scale of u_δ. Continuous random forcing therefore preferentially increases the subsurface amplitudes, since the energy flux from the surface causes a surface decay and a subsurface growth of u_δ. Using an observed wind stress series off Oregon and assuming that the wind was spatially uniform, the model predicted subsurface amplitudes of 5–9 cm s^{-1}, which are smaller than the observed amplitudes (~10–20 cm s^{-1}) by a factor of about 2.

Presumably the assumption of spatial uniformity should be abandoned if the model were to generate larger inertial oscillations. In the present work, the wind is assumed to be a "frozen" distribution moving toward the coast at a constant speed U. There is evidence to indicate that the inertial oscillations in the deep as well as coastal ocean are predominantly forced by propagating atmospheric disturbances (D'Asaro, 1985; Thomson and Huggett, 1981). The inviscid solution due to a *single* concentrated propagating front in an *unbounded* ocean was given by Kundu and Thomson (1985). The frequency was seen to be blue shifted, resulting in vertical dispersion. The subsurface energy, however, was rather small.

Obviously, much larger inertial oscillations can be generated by taking realistic wind profiles (having a *series* of propagating disturbances) and incorporating

a coast. The object of the present work is to extend the work of Kundu and Thomson so as to (i) include a coast, (ii) include superposition due to a series of propagating disturbances, and (iii) incorporate viscous damping. A model of coastal circulation due to fronts propagating away from the coast was given by Klinck et al. (1981), but the flow properties emphasized here were not studied. It will be seen that the effects of viscosity are small, but those due to superposition and presence of a coast are considerable; in fact, they increase the subsurface inertial oscillations to observed levels. However, the model oscillations are too highly correlated in the horizontal and vertical directions, much of which results from the assumed two-dimensionality.

2. Solution for a concentrated forcing

Consider a front propagating onshore in the x-direction at speed U over a coastal ocean on a flat shelf. The front and the coast are both aligned in the y-direction. The coordinates (x, y, z) and velocity components (u, v, w) are taken in the east, north (alongshore) and upward directions, respectively. The origin is placed at the surface–coast corner, with the ocean extending in the negative x-direction. The water depth is D, and the surface mixed layer depth is h. The subsurface water has a buoyancy frequency $N(z)$, and a vertical momentum and heat diffusivity ν. The ocean bottom is assumed slippery. Pressure and density perturbations from a state of rest are p and ρ, respectively.

The front is assumed infinitely long in the y-direction, so that the response is independent of y. The linearized equations of motion are taken to be

$$\left.\begin{aligned} u_t - fv &= -p_x + (\nu u_z)_z \\ v_t + fu &= (\nu v_z)_z \\ 0 &= -p_z - g\rho \\ u_x + w_z &= 0 \\ \rho_t - N^2 w/g &= (\nu\rho)_{zz} \end{aligned}\right\}, \tag{2}$$

where $\nu(z)$ is assumed to be inversely proportional to $N^2(z)$ in order that solutions can be found in terms of vertical normal modes (McCreary, 1981). The surface and bottom boundary conditions are

$$\left.\begin{aligned} &\nu u_z = \tau^x,\ \nu v_z = \tau^y,\ w = \rho = 0; \text{ at } z = 0 \\ &\nu u_z = \nu v_z = w = \rho = 0; \qquad \text{at } z = -D \end{aligned}\right\}. \tag{3}$$

Solutions to (2)–(3) can be found by expanding the variables in terms of the vertical normal modes $\psi_n(z)$ of the system:

$$(u, v, p) = \sum_{n=0}^{\infty} (u_n, v_n, p_n)\psi_n,$$

$$w = \sum_{n=0}^{\infty} w_n \int_{-D}^{z} \psi_n dz, \quad \rho = \sum_{n=0}^{\infty} \rho_n \psi_{nz}. \tag{4}$$

For $n \geq 1$, the vertical modes are given by

$$c_n^2\left(\frac{\psi_{nz}}{N^2}\right)_z + \psi_n = 0, \quad \text{subject to}$$

$$\psi_{nz} = 0 \quad \text{at} \quad z = 0, -D, \tag{5}$$

where c_n represents the long internal wave speed of the mode.

In the present model the wind forcing enters the ocean as a surface stress condition (3). However, it could also be introduced as a body force in a surface layer; in fact, that is the only way the forcing can be introduced in an inviscid model, as in Kundu and Thomson (1985). The two methods are equivalent if there is a surface mixed layer in which the body force can be assumed uniform. The mode shapes are depth-independent in the mixed layer, whose thickness also affects the values of c_n. They are normalized here such that $\psi_n(0) = 1$.

The modal coefficients satisfy

$$\left.\begin{aligned} (\partial_t + \nu_n)u_n - fv_n + p_{nx} &= \tau_n{}^x \\ (\partial_t + \nu_n)v_n + fu_n &= \tau_n{}^y \\ (\partial_t + \nu_n)p_n + c_n{}^2 u_{nx} &= 0 \\ c_n{}^2 w_n &= (\partial_t + \nu_n)p_n \\ \rho_n &= -p_n/g. \end{aligned}\right\}. \tag{6}$$

Here $\nu_n = \nu N^2/c_n{}^2$ is the viscous damping coefficient, and the coupling coefficients of each mode to the wind stress $\tau = (\tau^x, \tau^y)$ are

$$(\tau_n{}^x, \tau_n{}^y) = (\tau^x, \tau^y) \Big/ \int_{-D}^{0} \psi_n{}^2 dz. \tag{7}$$

The equation for u_n obtained from (6) is

$$(\partial_{tt} + f^2 + 2\nu_n\partial_t + \nu_n{}^2)u_n - c_n{}^2 u_{nxx} = \tau^x_{nt} + f\tau^y_n, \tag{8}$$

where a term $\nu_n\tau_n{}^x$ has been omitted on the right side to simplify the subsequent algebra. The maximum value of the neglected term with respect to the retained term is $\nu_n\tau_n{}^x/\tau^x_{nt} \sim 0.36$, assuming $n = 50$, $\nu = 1$ cm^2 s^{-1}, $N = 10^{-2}$ s^{-1}, $D = 250$ m, and a time scale of 2 h. The ratio is much smaller for the lower modes which dominate the solution, so that the omission of $\nu_n\tau_n{}^x$ is justified.

Equation (8) will be first solved for a "concentrated" line front moving over a coastal ocean, the forcing being taken to be

$$\tau_t{}^x + f\tau^y = U\tau_0\delta(x - Ut), \tag{9}$$

where $\delta(x)$ is the delta function. The solution u_δ to forcing (9) is therefore the impulse response, or the Green's function. In the absence of τ^y, (9) becomes $\tau_\xi{}^x = -\tau_0\delta(\xi)$, where $\xi = x - Ut$ is the moving coordinate. The forcing (9) then signifies that, across the front, τ^x undergoes a drop of τ_0 in space (in the moving coordinates), or an increase of τ_0 in time (in the fixed co-

ordinates). For an isolated front whose thickness is much less than the characteristic scale $2\pi U/f$ (~200 km) of the wave field, (9) is an adequate representation of the forcing (Kundu and Thomson, 1985). The solution for the general case of distributed forcing can be obtained by convolving the forcing with the impulse response.

For the nth mode, (9) becomes

$$\tau_{nt}^{x} + f\tau_n^{y} = U\tau_{0n}\delta(x - Ut), \tag{10}$$

where

$$\tau_{0n} = \tau_0 \Big/ \int_{-D}^{0} \psi_n^2 dz. \tag{11}$$

The solution to (8) due to forcing (10) will be denoted by $u_{n\delta}$, the subscript δ signifying that it is the field due to the impulsive forcing (10). It is written as the sum of the forced solution u_n' and a free solution u_n'', that is

$$u_{n\delta} = u_n' + u_n''. \tag{12}$$

Expressions for u_n' and u_n'' are derived below.

Forced Solution

The forced solution is the contribution in the absence of boundaries and is best obtained in terms of the coordinate system

$$\xi = x - Ut \tag{13}$$

fixed with the front. The field is steady in the moving frame of reference, and the equations of motion can be obtained by replacing ∂_t with $-U\partial_\xi$ in (8). For the forcing (10), this gives

$$u_{n\xi\xi}' - \left(\frac{2\nu_n U}{U^2 - c_n^2}\right)u_{n\xi}' + \left(\frac{f^2 + \nu_n^2}{U^2 - c_n^2}\right)u_n' = \frac{\tau_{0n}U\delta(\xi)}{U^2 - c_n^2}. \tag{14}$$

With common oceanographic parameter values the barotropic mode satisfies $U \ll c_0$; its contribution, however, is small and will be neglected. The baroclinic modes on the other hand satisfy $U > c_n$ so that no disturbance is felt ahead of the front (Geisler, 1970). The baroclinic solution of (14), subject to the radiation condition of $u_n' = 0$ for $\xi \geq 0$, is

$$u_n' = \frac{\tau_{0n}Ue^{a\xi}}{b}\left\{\sin k_n\xi \int_{\infty}^{\xi} e^{-a\xi}\cos k_n\xi\ \delta(\xi)d\xi - \cos k_n\xi \int_{\infty}^{\xi} e^{-a\xi}\sin k_n\xi\ \delta(\xi)d\xi\right\}, \tag{15}$$

which simplifies to

$$u_n' = -H(-\xi)b\tau_{0n}e^{a\xi}\sin k_n\xi, \tag{16}$$

where

$$k_n = \frac{f/U}{(1 - c_n^2/U^2)^{1/2}}\left[1 - \frac{\nu_n^2}{f^2}\frac{c_n^2/U^2}{1 - c_n^2/U^2}\right]^{1/2} \tag{17}$$

$$a = \frac{\nu_n/U}{1 - c_n^2/U^2} \tag{18}$$

$$b = \frac{1}{k_nU(1 - c_n^2/U^2)} \tag{19}$$

and $H(x)$ is the Heaviside unit function. As expected of Green's function, (16) has a discontinuity in the derivative of u_n' at $\xi = 0$. Equation (16) shows that the effect of viscosity ($a \neq 0$) is to cause a gradual decay of the solution behind the front. For $U = 400$ cm s^{-1} and the parameter values given later in Eq. (38), the e-folding decay scale a^{-1} is 2.4×10^5, 6.2×10^4 and 100 km for $n = 1$, 2 and 50, respectively. The viscous decay is therefore small for the low-order modes which dominate the solution.

The spectral characteristics of the inviscid version of (16) have been discussed in detail by Kundu and Thomson. In the presence of viscosity, (17) shows that the frequency of the nth mode in the fixed frame is

$$\omega_n = k_nU = \frac{f}{(1 - c_n^2/U^2)^{1/2}}\left[1 - \frac{\nu_n^2}{f^2}\frac{c_n^2/U^2}{1 - c_n^2/U^2}\right]^{1/2}. \tag{20}$$

For $U = 400$ cm s^{-1} and the parameter values (38), the viscous factor marked [ ]$^{1/2}$ in (20) is 1.000 for all the 50 modes used here. Therefore, viscosity hardly affects the frequency, which is blue shifted ($\omega_n > f$) as in the inviscid case. The blue shift decreases with the increase of n and U.

Free Solution

Equation (16) is the solution without boundaries, and the contribution u_n'' due to the presence of the coast is now added so that the total solution (12) satisfies the boundary condition

$$u_{n\delta} = 0 \quad \text{at} \quad x = 0. \tag{21}$$

It is easier to work with fixed coordinates (x, t) in deriving the coastal contribution. Suppose the front passes over the coast at $t = 0$. After a time t, the contribution at the coast due to the front is

$$u_n'(0, t) = b\tau_{0n}e^{-aUt}\sin(k_nUt), \tag{22}$$

which is obtained by substituting $\xi = -Ut$ in (16). To satisfy the boundary condition (21), the free solution must satisfy $u_n''(0, t) = -u_n'(0, t)$, so that

$$u_n''(0, t) = -b\tau_{0n}e^{-aUt}\sin(k_nUt). \tag{23}$$

The free solution u_n'' satisfies the homogeneous part of (8), whose Laplace transform gives

$$\tilde{u}_{nxx}'' - \frac{1}{c_n^2}[(s + \nu_n)^2 + f^2]\tilde{u}_n'' = 0, \tag{24}$$

where $\tilde{u}_n''(x, s)$ is the Laplace transform of $u_n''(x, t)$. The solution of (24) that is bounded at $x = -\infty$ is

$$\tilde{u}_n''(x, s) = A(s)e^{(x/c_n)[(s+\nu_n)^2+f^2]^{1/2}}. \tag{25}$$

Equation (25) shows that $A(s) = \tilde{u}_n''(0, s)$, which can be

obtained by taking the Laplace transform of (23). The inverse transform of (25) then gives $u_n''(x, t)$.

Total Solution

The total solution $u_{n\delta} = u_n' + u_n''$ is finally found to be

$$u_{n\delta}(x, t) = -H(Ut - x)\tau_{0n}be^{a(x-Ut)} \sin k_n(x - Ut)$$
$$- H\left(t + \frac{x}{c_n}\right)\tau_{0n}be^{-aU(t+x/c_n)}e^{\nu_n x/c_n}\sin k_n U(t + x/c_n)$$
$$- H\left(t + \frac{x}{c_n}\right)\tau_{0n}b\frac{xf^2}{c_n}$$
$$\times \left\{e^{-aUt}\sin k_n Ut\right\} * \left\{\frac{e^{-\nu_n t}J_1[f(t^2 - x^2/c_n^2)^{1/2}]}{(f^2t^2 - x^2/c_n^2)^{1/2}}\right\}, \quad (26)$$

where J_1 is the Bessel function, and the asterisk represents the convolution product of two functions delineated by braces, with the integral going from $-x/c_n$ to t. For example,

$$\{f(t)\} * \{g(t)\} \equiv \int_{-x/c_n}^{t} f(t - \alpha)g(\alpha)d\alpha. \quad (27)$$

In (26) the first term is the forced solution u_n', while the second and third terms constitute the free solution u_n''. The forced part propagates onshore at a fixed speed U, whereas the free parts propagate offshore at speed c_n. The fact that the forced part is nonzero even after the front moves over the land ($t > 0$) should not cause concern. For $t > 0$, the forced part makes the left side of (8) identically zero in the region of the flow, as can be verified by substitution.

Asymptotic form for small $x/c_n t$

The nature of the inviscid oscillations for values of $ft \to \infty$, holding xc_n/f fixed, can be derived from the inviscid form of the solution (26). By expanding the Laplace transform about the singularities in the complex s-place (Sutton, 1934), the asymptotic form is found to be

$$u_{n\delta} \sim -\frac{\tau_{0n}}{f(1 - c_n^2/U^2)^{1/2}}\left[2\sin\left(\frac{k_n x}{2}\right)\right.$$
$$\left. \times \cos\left(ft - \frac{k_n x}{2}\right) + \frac{xf}{c_n}\left(\frac{2}{\pi ft}\right)^{1/2}\cos\left(ft - \frac{\pi}{4}\right)\right]. \quad (28)$$

The second term in (28) denotes a decaying inertial oscillation near the coast, but the presence of the first term shows that inertial oscillations near the coast never die out completely for large times. This is unlike the case of a spatially uniform switched-on wind (Kundu et al., 1983), where all oscillations near the coast die out with time (coastal inhibition). The reason for this difference is that in the present case [see Eq. (26)] the forced solution keeps on impinging onto the coast; for the case of a switched-on uniform wind the forced part is nonpropagating. The fact that the inertial oscillations near the coast do not die out will be illustrated in the numerical evaluation of the solutions.

3. Considerations of distributed forcing

Note that the forcing (9) can also be written as

$$\tau_t^x + f\tau^y = \tau_0\delta(t - x/U) \quad (29)$$

for which the solution is u_δ, given by (26) and summed over the vertical normal modes. The field u_δ represents the flow due to a step change in τ^x. If, however, the gradients of τ^x are not like δ-functions (over a spatial scale of the "inertial wavelength" $\lambda_i = 2\pi U/f \sim 200$ km, or time scale of the inertial period $t_i \sim 15$ h) and/or the influence of τ^y is not negligible, then u_δ should only be regarded as the Green's function for the problem. In such a case the flow at a point $\mathbf{x} = (x, z)$ due to a propagating wind field can be written as the superposition

$$u(\mathbf{x}, t) = \int_0^{t-x/U} [\tau_t^x(\alpha) + f\tau^y(\alpha)]u_\delta(\mathbf{x}, t - \alpha)d\alpha, \quad (30)$$

where the entire wind field is assumed "frozen" and propagating at a uniform speed U. The discrete version of (30) is

$$u(\mathbf{x}, t) = \sum_{m=0}^{M} [\Delta\tau^x(m\Delta t) + f\Delta t\tau^y(m\Delta t)]u_\delta(\mathbf{x}, t - m\Delta t), \quad (31)$$

where Δt is the sampling interval, $\Delta\tau^x = \tau_{m+1}^x - \tau_m^x$, and $M\Delta t = t - x/U$. In (30) and (31), the time origin for the stress series $\tau(t)$ is chosen to be the leading edge of the stress.

To understand (31), consider only the τ^x component and assume that it can be idealized by a series of steps. This is shown in Fig. 1a, where the spatial distribution of stress is shown at $t = 0$. By superposition of steps the flow field for $t < x/U$ is zero, and for $t > x/U$ is

$$u(\mathbf{x}, t) = \Delta\tau^x(0)u_\delta(\mathbf{x}, t) + \Delta\tau^x(\Delta t)u_\delta(\mathbf{x}, t - \Delta t)$$
$$+ \cdots + \Delta\tau^x(M\Delta t)u_\delta(\mathbf{x}, x/U), \quad (32)$$

which is the same as (31). Note that the last term in (32) is not $\Delta\tau^x(t)u_\delta(\mathbf{x}, 0)$ as is usually the case in convolution sums, because nonzero values of u_δ start at the time $x/U < 0$ (Fig. 1b). Consequently, the upper limit in the integral (30) is not t, but $t - x/U$.

The superposition is expected to result in a growth of inertial oscillations. In fact, Kundu (1984) has shown that the rms amplitude grows at $t^{1/2}$ due to a forcing that has a white spectrum (that is, completely uncorrelated noise). It is now shown that the forcing spectrum need not be white for such a growth.

Let all spatial variations be suppressed, and denote the forcing as $\phi(t) \equiv \tau_t^x(t) + f\tau^y(t)$. Squaring and taking the expected value of (30) gives the variance at time t to be

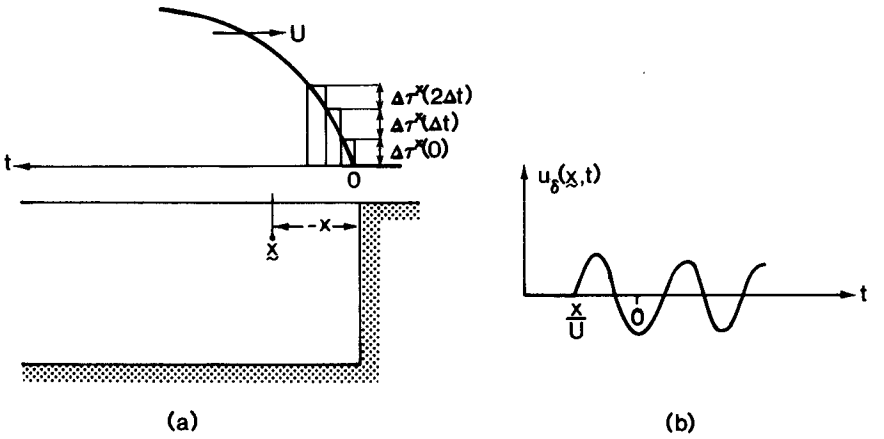

FIG. 1. (a) Illustration of the principle of superposition. A frozen profile of τ^x propagates at speed U. Values of stress changes at times 0, Δt and $2\Delta t$ are $\Delta\tau^x(0)$, $\Delta\tau^x(\Delta t)$ and $\Delta\tau^x(2\Delta t)$, respectively. (b) Typical impulse response at point x. Note that it starts at a negative time x/U.

$$\overline{u^2}(t) = \int_0^t \int_0^t \overline{\phi(\alpha)\phi(\beta)} u_\delta(t-\alpha) u_\delta(t-\beta) d\alpha d\beta. \quad (33)$$

Assume that the forcing has a stationary spectrum $S_\phi(\omega)$. Since S_ϕ is the Fourier transform of the autocorrelation, we have

$$\overline{\phi(\alpha)\phi(\beta)} = \int_{-\infty}^{\infty} S_\phi(\omega) e^{i\omega(\alpha-\beta)} d\omega. \quad (34)$$

Substitution of (34) into (33), and carrying out the integrations involving α and β, gives

$$\overline{u^2}(t) = \int_{-\infty}^{\infty} |\hat{u}_\delta|^2 S_\phi d\omega, \quad (35)$$

where $\hat{u}_\delta(\omega; t) = \int_0^t u_\delta(\alpha) e^{i\omega\alpha} d\alpha$ is the finite Fourier transform of u_δ for a record length t. Since $\hat{u}_\delta$ is peaked at $\omega = f$ (e.g., see Fig. 6 of Kundu, 1984), Eq. (35) shows that under stationary forcing only the near-inertial part of the wind spectrum generates inertial oscillations in the ocean. Moreover, when both τ^x and τ^y are present, the *clockwise* rotating near-inertial components of the wind dominate (Price, 1983). This can be seen most easily by taking an anticlockwise rotating stress vector of the form $\tau^x + i\tau^y = \exp(ift)$, for which the forcing $\tau_t^x + f\tau^y$ is identically zero.

Equation (35) was also derived in Kundu (1984), although in a less precise way. Furthermore, it was assumed there that the forcing spectrum is white, so that S_ϕ can be taken outside the integral in (35). This is really not necessary. Since $\hat{u}_\delta$ is sharply peaked near $\omega = f$, the forcing spectrum S_ϕ need only be "smooth" near $\omega = f$. Then (35) becomes approximately

$$\overline{u^2}(t) = S_\phi(f) \int_{-\infty}^{\infty} |\hat{u}_\delta|^2 d\omega \quad (36)$$

where $S_\phi(f)$ is the average value of the wind spectrum near the inertial frequency. Using Parseval's theorem (36) finally gives

$$\overline{u^2}(t) = 2\pi S_\phi(f) \int_0^t u_\delta^2 dt. \quad (37)$$

The rms amplitude therefore initially grows as $t^{1/2}$, and remains stationary for times larger than the decay time of u_δ.

The $t^{1/2}$ growth is valid if the forcing spectrum can be considered uniform within the bandwidth of $\hat{u}_\delta$. In the opposite extreme, if S_ϕ is so sharp at $\omega = f$ that it can be considered to be a δ-function, then it can be shown that (35) predicts the rms amplitude to increase linearly with time, which is the well-known resonant response of linear oscillators to a switched-on forcing.

Note that only smoothness of the wind spectrum near the inertial frequency is necessary for the $t^{1/2}$ growth; complete whiteness is not required. If, however, the wind spectrum were in fact white, then $S_\phi = \phi^2 \Delta t / 2\pi$ and (37) shows that $\overline{u^2}$ is also proportional to the step size Δt (as in random walk), provided of course that Δt is small enough to resolve the inertial period. Real winds, on the other hand, have a finite spectral width, and the sampling interval has to be chosen such that the Nyquist frequency $\pi/\Delta t$ is larger than the spectral width; in such a case S_ϕ (and hence the model inertial oscillations) is independent of Δt.

4. Results for coastal ocean

The following parameters are used for the coastal ocean:

$$\left.\begin{aligned} D &= 250 \text{ m} \\ h &= 25 \text{ m} \\ f &= 10^{-4} \text{ s}^{-1} \\ N &= 10^{-2} \text{ s}^{-1} \\ \nu &= 1 \text{ cm}^2 \text{ s}^{-1} \end{aligned}\right\} . \quad (38)$$

The mode shapes are obtained by solving the eigenvalue

problem (5). The eigenvalues for the first three modes are found to be $c_1 = 78$, $c_2 = 39$, and $c_3 = 26$ cm s^{-1}.

First a rather slow propagation speed of $U = 150$ cm s^{-1} is chosen. According to (20) the slow speed generates a large blue shift, so that a large flux of the inertial oscillations would be clearly visible in the solution. The Green's function u_δ is evaluated from (26) and (4), with $\tau_0 = 1$ dyn cm^{-2} and the constants defined in (11), (17), (18) and (19). It is found that 50 modes are sufficient for convergence of the sum (4). Taking $t = 0$ to be the instant the front crosses the coast, the flow field at each point (x, z) is evaluated from $t = -$(shelf width)$/U$ to $t = 25$ days, at intervals of 2 h. A time resolution of 10 min is used for evaluating the convolution integral in (26). The amplitude and phase of the inertial oscillations are found by complex demodulating the u field at the inertial frequency, using a bandpass filter to extract the inertial oscillations.

Figure 2 shows the amplitude at several depths when no coast is present. In this case the flow field at any depth is a function of the moving coordinate ξ alone, and the horizontal axis in Fig. 2 can be taken as either ξ/λ_i in the moving frame or t/t_i in the fixed frame. The viscid flow field in Fig. 2 is seen to be very similar to the inviscid field described in details by Kundu and Thomson, confirming the smallness of viscous effects on inertial oscillations. The field is seen to be intermittent, the dominant period of the intermittancy being $2\pi/(\omega_1 - f) = 5.8t_i$ (Gill, 1984; Kundu and Thomson, 1985). At a typical subsurface depth of 90 m, the maximum amplitude is 1.2 cm s^{-1}. Larger amplitudes are reached at the bottom, a feature also seen in the solutions of Gill (1984). In fact, both maximum and minimum amplitudes occur on a slippery flat bottom, where $\psi_{nz} = 0$. With some exceptions (e.g., Saunders, 1983; Sanford, 1975), bottom intensification of inertial oscillations is not a commonly observed feature, presumably due to the existence of a viscous-bottom boundary layer.

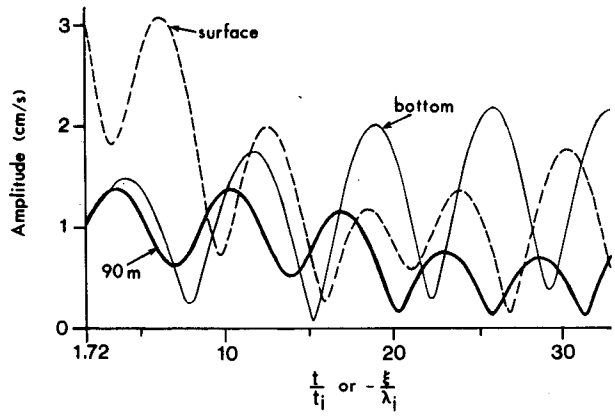

FIG. 2. Amplitude of inertial oscillation at three depths due to a concentrated forcing of $\Delta\tau^x = 1$ dyn cm^{-2}. Shallow water parameters (38) are used, along with $U = 150$ cm s^{-1} and no coast. The time axis starts at $t = 1.72t_i$ due to the loss of record length caused by the demodulation filter. Note that the minimum amplitude at the surface occurs first, followed by the maximum at 90 m, and then the maximum at the bottom. This is due to the finite downward speed of energy propagation.

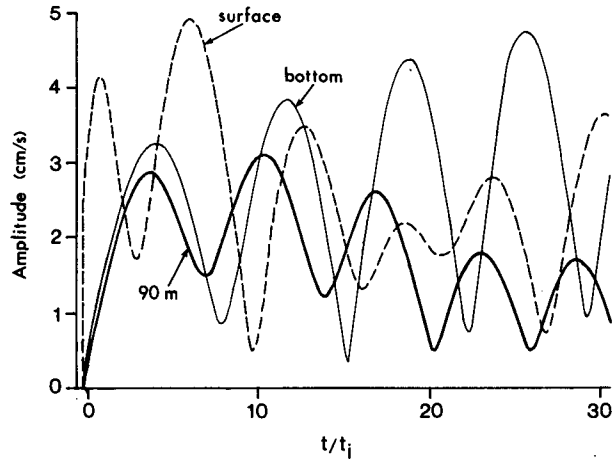

FIG. 3. Amplitude of inertial oscillations at $x = -17.3$ km for three values of depth due to a concentrated forcing of $\Delta\tau^x = 1$ dyn cm^{-2}. Shallow water parameters (38) are used, along with $U = 150$ cm s^{-1} and the presence of a coast. Comparing with Fig. 2, note that the presence of a coast has increased the subsurface oscillations.

Figure 3 shows the behavior of the amplitude at $x = -17.3$ km for several values of depth, when a coast is introduced at $x = 0$. The maximum amplitude at 90 m is now 3 cm s^{-1}, and bigger values are again achieved at the bottom. Comparison with Fig. 2 shows that the presence of the coast has obviously intensified the inertial oscillations at this offshore position. The oscillations much closer to the coast are, however, smaller. The initial gain of subsurface inertial energy can be traced to the flux of energy from the surface–coast corner. This is shown in Fig. 4, which shows the contours of amplitude at several times. A region of amplitude greater than 2 cm s^{-1} is seen to descend from the surface–coast corner, signifying a downward flux, as in the case of the switched-on uniform wind (Kundu et al. 1983). Unlike the switched-on case, however, the amplitude near the coast does not monotonically decay, in agreement with the asymptotic form (28). Another region of gain appears near the bottom at $x \sim -25$ km, presumably due to the bottom reflection of some of the relatively higher frequency components. At the large time of $t/t_i = 27.4$, Fig. 4 shows a pattern of highs separated by about 50 km. This is in rough agreement with the asymptotic form (28), in which the first term shows that the large amplitudes should be separated by a length $2\pi/k_n$, which is 75 km for $n = 1$ and 90 km for very high-order modes.

The above results indicate that the propagation of a

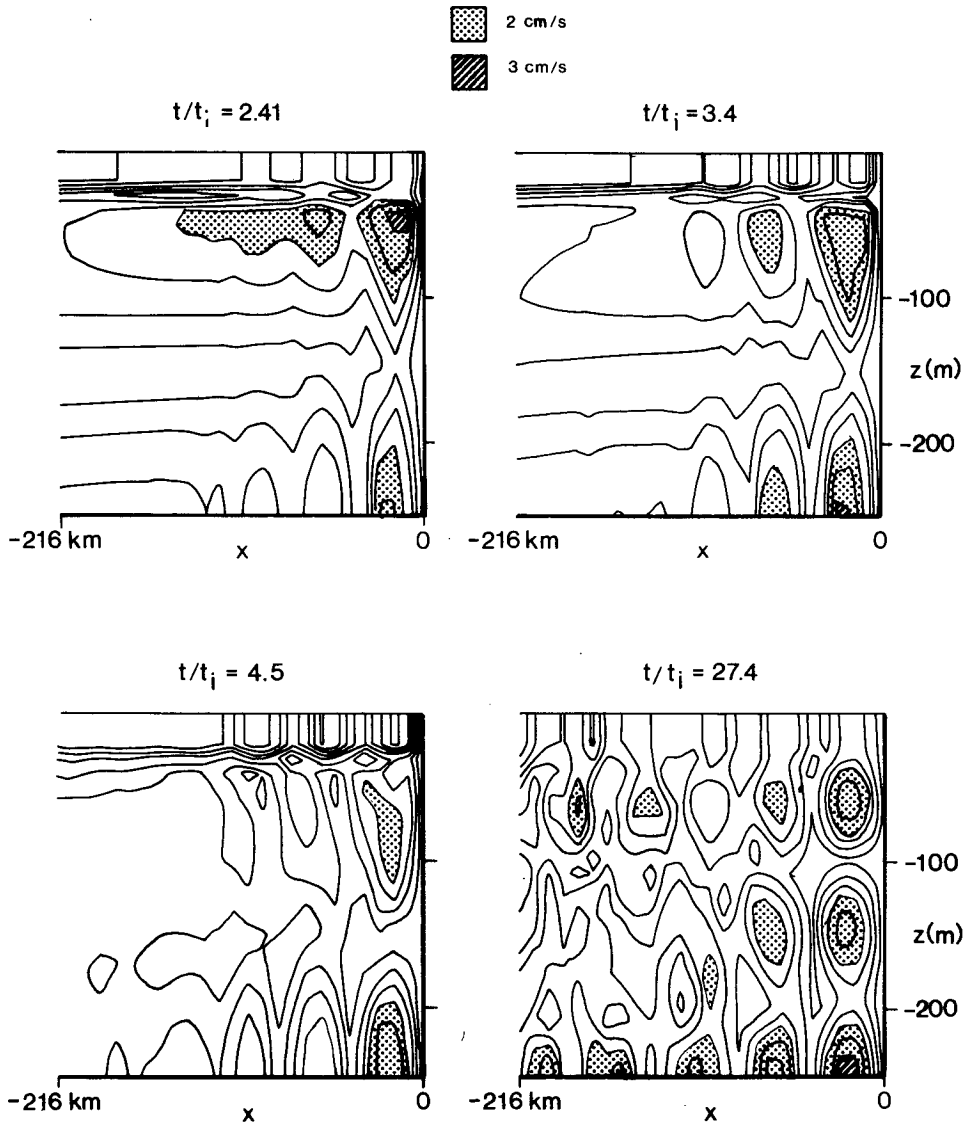

FIG. 4. Contour plots of inertial amplitudes for four values of t/t_i for the calculation shown in Fig. 3. Contour interval is 0.5 cm s^{-1}. Regions of subsurface amplitude greater than 2 cm s^{-1} are shaded, and those greater than 3 cm s^{-1} are hatched. Note the descent of a region greater than 2 cm s^{-1} from the surface–coast corner, the absence of a complete decay near the coast, and a regular series of highs in x for large times.

front, having a discontinuity of $\Delta\tau^x = 1$ dyn cm^{-2}, over a coastal ocean produces inertial oscillations that are larger in magnitude than those obtained in either the switched on case (Kundu et al., 1983) or in the boundary-free case (Kundu and Thomson, 1985). It is now shown that much larger oscillations are generated by superposing solutions due to a series of propagating disturbances.

In order to determine the oscillations due to a realistic forcing, the wind stress observed off the coast of British Columbia in the summer of 1977 is used next. Measurements at several coastal and oceanic stations showed that the wind propagated toward the coast in frontlike disturbances aligned alongshore (Thomson and Huggett, 1981). The passage of warm fronts caused a sudden veering of the wind from southeasterly to southwesterly; these are marked by arrows in Fig. 5. The speed of propagation was $U = 400$ cm s^{-1}. Starting on 21 June, large inertial oscillations (30–50 cm s^{-1}) were observed in the upper 20 m, whereas those below the surface were much smaller ($\sim$5 cm s^{-1}).

Since a detailed simulation is not the purpose of the paper, the observed density field is not used here. Instead the parameters (38) are used, along with $U = 400$

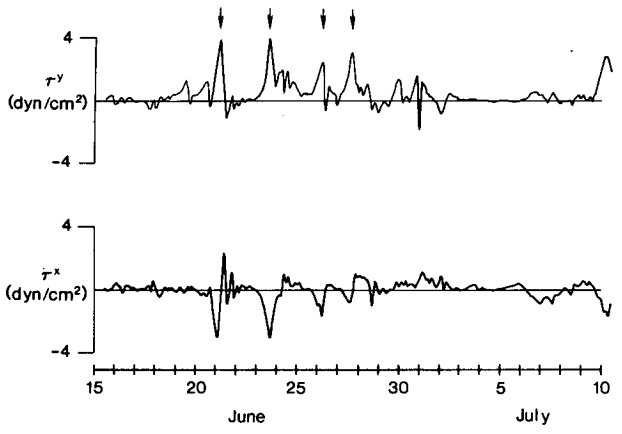

FIG. 5. Wind stresses measured by Thomson and Huggett (1981) off the coast of British Columbia. Arrows mark the positions of fronts across which the wind suddenly veered from southeasterly to southwesterly. These fronts were observed to move onshore at $U = 400$ cm s^{-1}.

cm s^{-1}. Figure 6 shows the amplitude variation at $x = -46$ km. The surface values reach 60 cm s^{-1}, whereas the mid-depth values are less than 15 cm s^{-1}. The fact that the subsurface amplitudes are now much smaller than the surface values is due to the larger propagation speed of the forcing. With $U = 400$ cm s^{-1}, the first three modal frequencies are $\omega_1 = 1.020f$, $\omega_2 = 1.005f$, and $\omega_3 = 1.002f$. The small blue shift results in only a small downward energy flux.

The correlation and phase difference of velocity vectors are most easily determined by evaluating the complex correlation coefficient

$$\mathbf{R} = \frac{\overline{\mathbf{w}^\dagger(\mathbf{x}_0, t)\mathbf{w}(\mathbf{x}, t)}}{[\overline{\mathbf{w}^\dagger(\mathbf{x}_0, t)\mathbf{w}(\mathbf{x}_0, t)}]^{1/2}[\overline{\mathbf{w}^\dagger(\mathbf{x}, t)\mathbf{w}(\mathbf{x}, t)}]^{1/2}}, \quad (39)$$

where $\mathbf{w} = u + iv$, $\mathbf{x}_0$ and $\mathbf{x}$ are the two locations, and $(\ )^\dagger$ denotes complex conjugation. The magnitude of $\mathbf{R}$ gives a *weighted* average correlation, and the phase angle of the complex number $\mathbf{R}$ gives the average counterclockwise angle of vector at $\mathbf{x}$ with respect to the vector at $\mathbf{x}_0$. Figure 7 shows the horizontal distribution of correlation of the surface currents of Fig. 6. The correlation magnitude is high, and the phase distribution corresponds to an onshore propagation with horizontal wavelength of 248 km, close to the inertial wavelength of $2\pi U/f = 251$ km. Therefore the effect of the coastline on the horizontal phase variation of currents is small, as observed by Thomson and Huggett (1981) and Kundu and Thomson (1985). This, however, is not true very close to the coastline, where Fig. 7 shows a flattening out of the phase. The correlation of the subsurface currents is qualitatively similar to that of the surface currents and is not shown.

The vertical distribution of correlation of the same currents is shown in Fig. 8. The distribution at $x = -46$ km is shown, but those at other offshore locations are qualitatively similar. The current vectors are seen to be highly correlated in the vertical, and rotate clockwise with depth with an implied upward phase speed of $c_z = 0.6$ cm s^{-1}, which is of the order of the observed values.

It is not difficult to see why the model oscillations should be so highly correlated both horizontally and vertically even for a stochastic forcing. The high correlation in fact results from the high correlation of the $\mathbf{w}_\delta(\mathbf{x}, t)$ field itself (where $\mathbf{w}_\delta = u_\delta + iv_\delta$), and the fact that the same wind field passes over all the horizontal locations. The latter fact would have produced a perfect horizontal correlation were it not for the presence of the waves reflected off the coast. The high vertical cor-

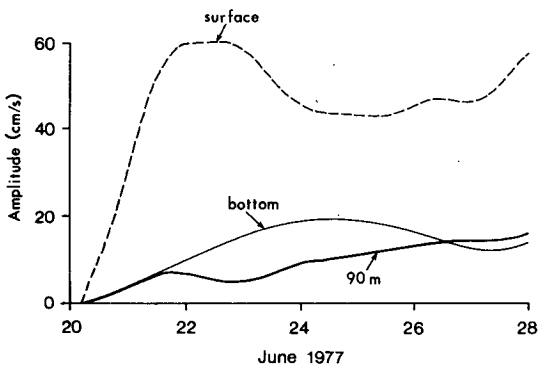

FIG. 6. Amplitude of inertial oscillations at $x = -46$ km for three values of depth, forced by the late June event of Fig. 5. Shallow water parameters (38) are used, along with $U = 400$ cm s^{-1} and the presence of a coast.

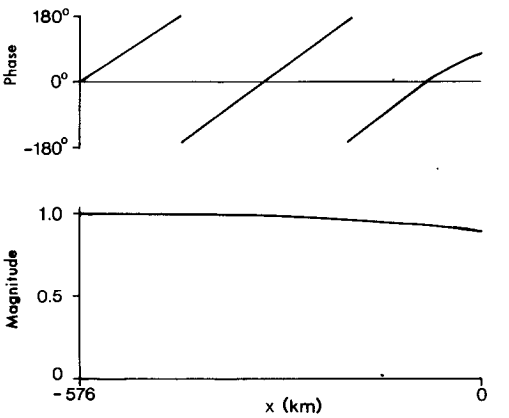

FIG. 7. Horizontal distribution of magnitude and phase angle of correlation of the surface currents forced by the late June event of Fig. 5. Shallow water parameters (38) are used, along with $U = 400$ cm s^{-1} and the presence of a coast. The correlation is computed with respect to the offshore location $x = -576$ km. Note the high correlation magnitude and the counterclockwise rotation of velocity vectors with onshore distance corresponding to a horizontal wavelength of 248 km.

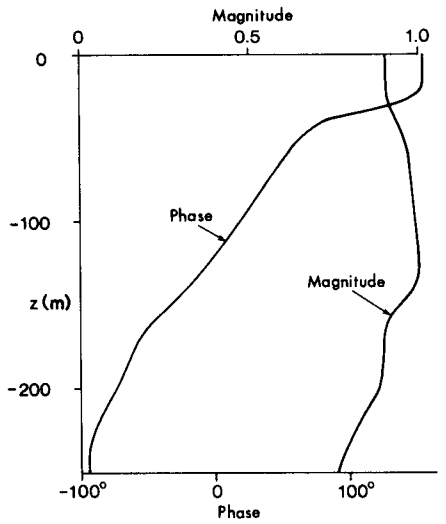

FIG. 8. Vertical distribution of magnitude and phase angle of correlation of the currents (at $x = -46$ km) forced by the late June event of Fig. 5. Shallow water parameters (38) are used, along with $U = 400$ cm s^{-1} and the presence of a coast. The correlation is computed with respect to the depth 120 m. Note the high correlation magnitude, and the clockwise rotation of velocity vectors with depth.

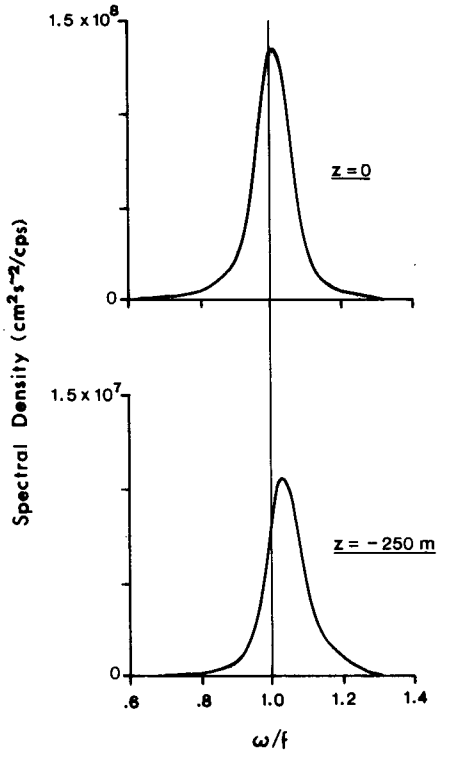

FIG. 9. High resolution spectra of u forced by the late June event of Fig. 5. Surface and bottom spectra at $x = -46$ km are shown, with a bandwidth of $0.015f$. Shallow water parameters (38) are used, along with $U = 400$ cm s^{-1} and the presence of a coast. Note the increase of blue shift with depth and the fact that the presence of the coast causes the blue shift at the bottom (~5%) to be larger than that of the first mode (~2%).

relation is due to the domination of a few low-order modes in the solution.

High resolution spectra of the surface and bottom currents at $x = -46$ km are shown in Fig. 9. The increase of the blue shift with depth is due to the rapid downward leakage of the low-order modes. The spectra have a single peak because the ω_n are too close together for the rather high assumed value of $U/c_1 = 5.1$. These facts have been pointed out in the coast-free calculations of Kundu and Thomson. The interesting new feature in Fig. 9 is that the bottom spectrum has at least a 5% blue shift, whereas the largest modal frequency is only $\omega_1 = 1.02f$. The higher blue shift is due to the presence of the coast, and enters the model through the Bessel function terms in (26).

Figure 10 shows a calculation using the smaller value of $U = 150$ cm s^{-1}. This figure should be compared with Fig. 6 where $U = 400$ cm s^{-1}; all other parameters are identical for the two figures. The mid-depth maximum amplitudes in Fig. 10 are about four times those in Fig. 6. Substantial near-inertial oscillations can therefore be generated by realistic wind fields translating at slower speeds.

A check was made on the validity of (37), which says that the inertial energy in the ocean should be proportional to $S_\phi(f)$. The calculation of Fig. 10 was repeated after subtracting out the inertial components of the wind by bandpass filtering. The resulting wind stress series decreased in rms value by about 15%, and visually it looked surprisingly similar to the original series shown in Fig. 5. However, the model inertial amplitudes driven by this wind decreased by a factor of 6! A second check was to compare the model amplitudes with those predicted from (37). The spectrum S_ϕ of the forcing series $\phi(t) \equiv \tau_i^x(t) + f\tau^y(t)$ was computed, and its value near $\omega = f$ was found to be $S_\phi(f) \sim 5 \times 10^{-5}$ cm^4 s^{-5}. From Fig. 3, the average amplitude of u_δ at 90 m is 2 s cm^{-1}. (The unit of u_δ is that of velocity per

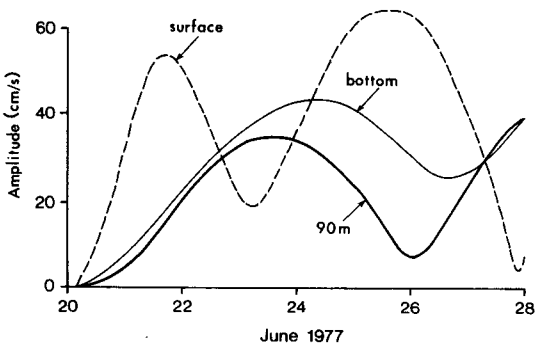

FIG. 10. As in Fig. 6 except $U = 150$ cm s^{-1}. Note that the subsurface amplitudes are now about four times larger.

unit stress; this gives s cm^{-1}.) Equation (37) then predicts the average amplitude after eight days to be 30 cm s^{-1}, which is close to the model value in Fig. 10.

5. Results for deep ocean

A calculation in the deep ocean, without the presence of the coast, is now performed. The parameters used are

$$\left.\begin{aligned} D &= 2500 \text{ m} \\ h &= 50 \text{ m} \\ f &= 10^{-4} \text{ s}^{-1} \\ \rho_0 &= \begin{cases} 1, & z > -h \\ 1 + \Delta\rho_1[1 - e^{(z+h)/b_1}] & \\ \quad + \Delta\rho_2[1 - e^{(z+h)/b_2}], & z < -h \end{cases} \\ \nu_{\min} &= 0.1 \text{ cm}^2 \text{ s}^{-1} \\ U &= 600 \text{ cm s}^{-1}, \end{aligned}\right\} \quad (40)$$

where $\Delta\rho_1 = 0.00125$ gm cm^{-3}, $b_1 = 200$ m, $\Delta\rho_2 = 0.00225$ gm cm^{-3}, and $b_2 = 1000$ m. Both the ocean and the mixed layer depths in (40) are larger than the ones in (38) used for coastal calculations. The background density profile ρ_0 (Fig. 11) has a thermocline just below the mixed layer with $N^2_{\max} = 0.8 \times 10^{-4}$ s^{-2}. The vertical viscosity at the mixed layer base is taken as 0.1 cm^2 s^{-1}, and because of the assumed N^{-2} behavior its value at a depth of 1000 m is about 1 cm^2 s^{-1}. The wind translation speed is chosen to be of the order of hurricane motions (Price, 1983).

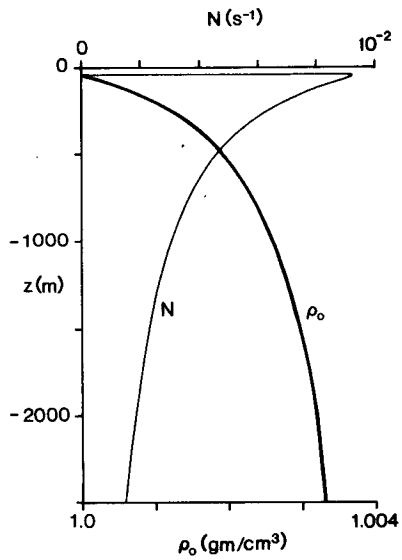

FIG. 11. Vertical distributions of background density and the associated buoyancy frequency used in the open ocean calculations.

Calculation of the vertical modes gives the first three eigenvalues to be $c_1 = 253$, $c_2 = 132$, and $c_3 = 88$ cm s^{-1}. The corresponding modal frequencies are $\omega_1 = 1.103f$, $\omega_2 = 1.025f$, and $\omega_3 = 1.011f$. For a fixed value of U, the blue shifts are larger in the deep ocean because of the larger values of c_n. A substantial downward flux can therefore be expected even at large values of U.

As an example, the wind field of Fig. 5 during 15 June–10 July (25 days) is used as forcing. Because of the long times required for dispersion in the deep open ocean (Gill, 1984), the subsurface oscillations here can be made up of responses to wind events that took place months ago. That is why the model results in this section are forced by a 25-day long segment of Fig. 5, as opposed to an 8-day long segment for coastal calculations.

The resulting contours of $u(z, t)$ in the upper 1000 m of the ocean are shown in Fig. 12. The phases are seen to propagate upward with an average speed of $c_z \sim 2$ cm s^{-1}. The oscillations decrease in magnitude with depth, which is more clearly seen in the amplitude plot of Fig. 13. The maximum subsurface amplitudes at 80, 160, 280 and 1000 m are 23, 14, 7 and 3 cm s^{-1} respectively. When the calculation is stopped on 10 July, the subsurface magnitudes are still increasing due to the downward flux from the surface. The surface magnitudes seem to have reached an equilibrium between the leakage and wind forcing. The subsurface amplitudes clearly show that the peaks and valleys occur at progressively increasing times with increasing depths. The implied speed of downward propagation of energy is 0.2 cm s^{-1} in the upper thermocline, and rapidly decreases below.

The spectra at two depths (Fig. 14) show that the blue shift of the primary peak increases with depth, and that there is a secondary peak at the first mode frequency $\omega_1/f = 1.1$. The presence of a secondary peak in Fig. 14, but not in Fig. 9, is due to the fact that U/c_1 is much smaller for the assumed deep water parameters, resulting in a large $\omega_1 - f$ (see Kundu and Thomson for further explanation).

Calculations of the correlation showed that the currents were highly correlated in the horizontal as well as in the vertical.

6. Summary and conclusion

A linear, two-dimensional, continuously stratified model has been developed to study the inertial oscillations generated by a propagating wind field. The model is an extension of the one in Kundu and Thomson (1985) to include viscous damping, presence of a coast, and superposition due to a distributed forcing. It has been shown that the effects of viscous damping on inertial oscillations are small, but the effects of coastline and superposition are considerable in that

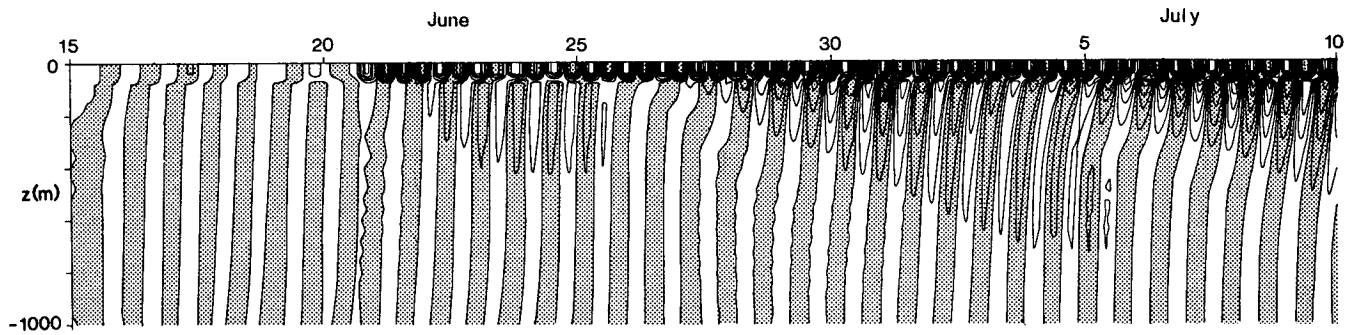

FIG. 12. Contour plots of $u(z, t)$ in the open ocean calculation. Parameters used are (40), and the forcing is the wind series of Fig. 5. Note the upward phase propagation.

much larger subsurface inertial oscillations are generated. Essentially, the coast generates an additional blue shift, and superposition of responses with random phase does not cancel out but increases the rms value as the square root of the number of additions. The forcing spectrum need not necessarily be white for this behavior, only that it should be "smooth" near the inertial frequency, since only this part of the forcing spectrum contributes. In a linear model, very little inertial oscillations are generated if the near-inertial components of the wind are removed by bandpass filtering, although this may have reduced the rms value of the wind variation by only a small amount.

Calculation of a concentrated front in shallow water (D = 250 m) at a slow propagation speed (U = 150 cm s^{-1}) is performed to illustrate the increase of the subsurface oscillations due to the presence of a coast (Figs. 2 and 3). The increase is caused by a downward flux from the surface–coast corner (Fig. 4). When the coastal model is forced by an 8-day long segment of an observed wind (Fig. 5) propagating at U = 400 cm s^{-1}, the maximum mid-depth model amplitudes reached are about 15 cm s^{-1}, and the surface values are nearly 60 cm s^{-1} (Fig. 6). These values are of the order of those observed by Thomson and Huggett (1981), except that the model subsurface currents are larger than the observed currents, many of which were clearly within the bottom boundary layer.

The model shows that the blue shift, and hence the subsurface amplitudes, increase with c_1/U. Since c_1 is larger in the deep ocean than in shallow water, it follows

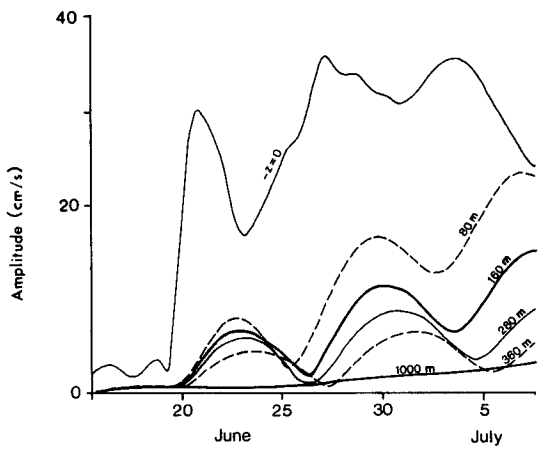

FIG. 13. Amplitude variation at several depths in the open ocean calculation. Parameters used are (40), and the forcing is the wind series of Fig. 5. Note that the peaks propagate downward at 0.2 cm s^{-1}.

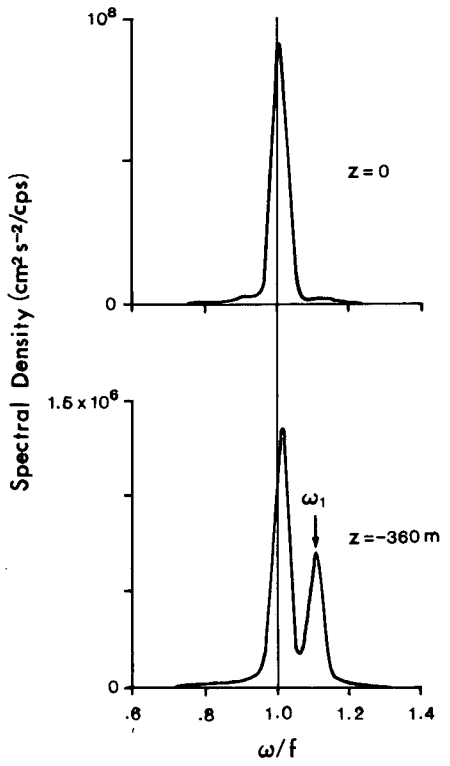

FIG. 14. High resolution spectra of u in the open ocean calculation. Parameters used are (40), and the forcing is the wind series of Fig. 5. Note the secondary peak at ω_1 and the increase of the blue shift of primary peak with depth.

that large downward fluxes of inertial energy can be generated there. In one calculation a deep ocean (D = 2500 m) with a thermocline is forced by a 25-day long segment of coastally observed wind series (Fig. 5), assumed to propagate at U = 600 cm s^{-1}. The model subsurface maximum amplitudes decrease with depth from 23 cm s^{-1} at 80 m to 3 cm s^{-1} at 1000 m. A decrease with depth is universally observed in deep water data. The observed amplitudes can sometimes be as large as 6–7 cm s^{-1} even below 2000 m (Leaman and Sanford, 1975; Sanford, 1975; D'Asaro and Perkins, 1984). Clearly the model is able to generate these large deep water observations, since in the open ocean the propagating wind events are frequently composed of stresses of order 10–20 dyn cm^{-2} (D'Asaro, 1985; Price, 1983), several times larger than the maximum stresses (<5 dyn cm^{-2}) used in the model. Moreover, it is important to note that much larger oscillations could be generated in the model simply by forcing it for a longer time, because the decay time of the impulse response u_δ is several months long (see also Gill, 1984).

The spectra (Fig. 9, Fig. 14) show a primary peak whose blue shift increase with depth. This is in agreement with several observations (e.g., Fig. 5 of Fu, 1981; Millot and Crépon, 1981; Price, 1983) and is due to a smaller contribution of the high-order modes with depth. The spectra can also have a secondary peak at ω_1 if U/c_1 is not too large (Fig. 14), and such "split" inertial peaks are frequently observed (Fu, 1981; Kundu, 1976).

In spite of the above successes the model has major faults. The model oscillations are too highly correlated, both vertically and horizontally. A stochastic forcing, if assumed frozen and simply horizontally advected, does not generate high intermittency or low coherence. The model intermittency is dominated by the phase mixing of the various modes [resulting in a dominant periodicity of $2\pi/(\omega_1 - f)$ for the amplitude], rather than the phase mixing of the responses to the various segments of the wind series.

Many of the above deficiences no doubt result from the assumed two-dimensionality and the neglect of the β-effect. Realistic storms and the associated fronts are localized in space, and the propagation and dispersions perpendicular to the direction of translation are important. The various storms and the associated fronts have different tracks and different speeds of propagation. The wave groups therefore also propagate meridionally as they descend from the surface, and the ones propagating poleward turn equatorward at their critical latitudes (Munk and Phillips, 1968; Fu, 1981; Gill, 1984). Some calculations suggest that the conversion of inertial oscillations to high frequency internal waves by nonlinear interactions is small (McComas and Müller, 1981). Recent work also suggests that the benthic boundary layer is a good reflector of inertial waves (Fu, 1981; D'Asaro, 1982). It would therefore seem that the inertial waves can travel thousands of kilometers before being dissipated, and the oscillations at a subsurface point could really be made up of the responses to entirely different storms. Along the way the waves could be distorted by numerous factors. For example, the mean motion could trap, focus or amplify these waves (Kunze, 1985; Weller, 1982). The superposition of such oscillations would definitely be far more incoherent than the ones generated in the present two-dimensional model.

The present work does nevertheless show that the wind forcing could explain the observed levels of subsurface inertial energy. Wave–wave interactions or other mechanisms need not necessarily be responsible. The fact that the internal wave spectrum is vertically asymmetric for near-inertial frequencies with predominantly downward energy propagation, although it is vertically symmetric for $\omega \gg f$, must indicate that the inertial oscillations are predominantly surface forced by the wind. Work on the wind forcing should therefore continue, and it is hoped that a three-dimensional model be soon developed to study propagating disturbances.

Acknowledgments. The work was supported by NSF Grant OCE-8509228. Computing time on CRAY-1 was donated by the National Center for Atmospheric Research, Boulder, Colorado. I am grateful to Julian P. McCreary for helpful discussions, and to Eric Kunze, David Rubenstein and Richard E. Thomson for comments on the manuscript. I thank Kevin Kohler for computer programming, and Kathy Maxson for drafting and typing.

REFERENCES

D'Asaro, E. A., 1982: Absorption of internal waves by the benthic boundary layer. *J. Phys. Oceanogr.*, **12,** 323–336.

——, 1985: The energy flux from the wind to near-inertial motions in the surface mixed layer. *J. Phys. Oceanogr.*, **15,** 1043–1059.

——, and H. Perkins, 1984: A near-inertial internal wave spectrum for the Sargasso Sea in late summer. *J. Phys. Oceanogr.*, **14,** 489–505.

Fu, L. L., 1981: Observations and models of inertial waves in the deep ocean. *Rev. Geophys. Space Phys.*, **19,** 141–170.

Geisler, J. E., 1970: Linear theory of the response of a two-layer ocean to a moving hurricane. *Geophys. Fluid Dyn.*, **1,** 249–272.

Gill, A. E., 1984: On the behavior of internal waves in the wakes of storms. *J. Phys. Oceanogr.*, **14,** 1129–1151.

Klinck, J. M., L. J. Pietrafesa and G. S. Janowitz, 1981: Continental shelf circulation induced by a moving, localized wind stress. *J. Phys. Oceanogr.*, **11,** 836–848.

Kundu, P. K., 1976: An analysis of inertial oscillations observed near Oregon coast. *J. Phys. Oceanogr.*, **14,** 1901–1913.

——, 1984: Generation of coastal inertial oscillations by time varying wind. *J. Phys. Oceanogr.*, **14,** 1901–1913.

——, and R. E. Thomson, 1985: Inertial oscillations due to a moving front. *J. Phys. Oceanogr.*, **15,** 1076–1084.

——, S-Y. Chao and J. P. McCreary, 1983: Transient coastal currents and inertio-gravity waves. *Deep-Sea Res.*, **30,** 1059–1082.

Kunze, E., 1985: Near-inertial wave propagation in geostrophic shear. *J. Phys. Oceanogr.*, **15,** 544–565.

Leaman, K. D., and T. B. Sanford, 1975: Vertical energy propagation

of inertial waves: A vectorspectral analysis of velocity profiles. *J. Geophys. Res.*, **80,** 1975–1978.

McComas, C. H., and P. Müller, 1981: Time scales of interactions among oceanic internal waves. *J. Phys. Oceanogr.*, **11,** 139–147.

McCreary, J. P., 1981: A linear stratified ocean model of the equatorial undercurrent. *Phil. Trans. Roy. Soc. London,* **2198,** 603–635.

Millot, C., and M. Crépon, 1981: Inertial oscillations on the continental shelf of the Gulf of Lions: Observations and theory. *J. Phys. Oceanogr.*, **11,** 639–657.

Munk, W., and N. Phillips, 1968: Coherence and band structure of inertial motion in the sea. *Rev. Geophys.*, **6,** 447–471.

Pollard, R. T., 1970: On the generation by winds of inertial waves in the ocean. *Deep-Sea Res.*, **17,** 795–812.

Price, J. F., 1983: Internal wave wake of a moving storm. Part I: Scales, energy budget and observations. *J. Phys. Oceanogr.*, **13,** 949–965.

Sanford, T. B., 1975: Observations of the vertical structure of internal waves. *J. Geophys. Res.*, **80,** 3861–3871.

Saunders, P. M., 1983: Benthic observations on the Madeira Abyssal Plain: Currents and dispersion. *J. Phys. Oceanogr.*, **13,** 1416–1429.

Sutton, W. G. L., 1934: The asymptotic expansion of a function whose operational equivalent is known. *J. London Math. Soc.*, **9,** 131–137.

Thomson, R. E., and W. S. Huggett, 1981: Wind-driven inertial oscillations of large spatial coherence. *Atmos. Ocean,* **19,** 281–306.

Weller, R. A., 1982: The relation of near-inertial motions observed in the mixed layer during the JASIN (1978) experiment to the local wind stress and to the quasi-geostrophic flow field. *J. Phys. Oceanogr.*, **12,** 1122–1136.